Tree Detection and Delineation from LiDAR point clouds using RANSAC

Peter Tittmann[1], Sohail Shafii[2], Bruce Hartsough[3], Bernd Hamann[4]
[1]Department of Geography, UCD (University of California, Davis),
ptittmann@gmail.com
[2]Department of Computer Science, UCD, ssshafii@ucdavis.edu
[3]Department of Biological and Agricultural Engineering,
UCD, brhartsough@ucdavis.edu
[4]Department of Computer Science, UCD, hamann@cs.ucdavis.edu

Abstract

As Light Detection And Ranging (LiDAR) (point) data sets increase in resolution, earth scientists become more interested in detecting and delineating trees using LiDAR. The majority of conventional methods which detect and delineate trees convert point data into gridded surfaces. Unfortunately, this conversion process has the potential to introduce error. We improve a point-based geometric model fitting strategy based on RANdom Sample Consensus (RANSAC), known as *StarSac*, and compare the method's results against field data. The analysis demonstrates that *StarSac* produces similar results to field data, and is a strong alternative to conventional methods.

Keywords: geometric, RANSAC, model fitting

1. Introduction

As the capabilities of aerial Remote Sensing (RS) technologies such as Light Detection And Ranging (LiDAR) increase in precision, the potential to directly measure vegetation characteristics has increased as well. The majority of methods using LiDAR data for individual tree detection and delineation emphasize the conversion of point data into gridded surfaces, and the application of algorithmic tools widely used for terrain surface analysis to identify and delineate individual trees. While these methods have been shown to be effective under a range of circumstances, the conversion to gridded data followed by watershed, valley-following, or other such methods have the potential to introduce error from both steps. Surface interpolation from unstructured point data (i.e., not evenly distributed in coordinate space) is non-trivial, requiring arbitrary decisions about cell size and interpolation strategy. Equally, strategies for delineating individual trees from gridded data are subject to error resulting from application of algorithms designed to function on terrain surfaces to idiosyncratic forest canopy surfaces. As these steps are sequential, errors from the first step can be compounded in the second. To reduce the impact of such errors, methods are often parameterized by field data (species, canopy height, etc.) and as a result can be quite accurate in tree detection and delineation. If extensive field data collection is required to parameterize the algorithm, the efficiency of the inventory effort is compromised.

We have developed a RANdom SAmple Consensus (RANSAC)-based (Fischler and Bolles 1981) program, henceforth referred to as *StarSac*, which uses a geometric model fitting strategy to identify individual tree crowns directly from point data. Basal area is then calculated using a regression relating Diameter at Breast Height (DBH) to total height. We identify the location, and height of all trees within the scene without parameterization from field data using the point data directly and avoid the compounding error problem described above. Field data is used to parameterize the height-DBH regression for estimation of Diameter at Breast Height (1.37) (DBH).

1.1 Study site

The study site is the *van Eck forest*, consisting of 879 ha of mixed conifer forestland in Humboldt County, California. The van Eck forest contains a great deal of structural and successional diversity, including riparian areas, selectively logged second growth mixed conifer stands, and stands which have not been harvested since initial clear cut in the early part of the century.

The forest is divided in to four tracts, ranging from 130 ha to 315 ha (See Figure 1). It is a well-stocked second growth forest with an average timber volume of 170 m^3ha^{-1}.

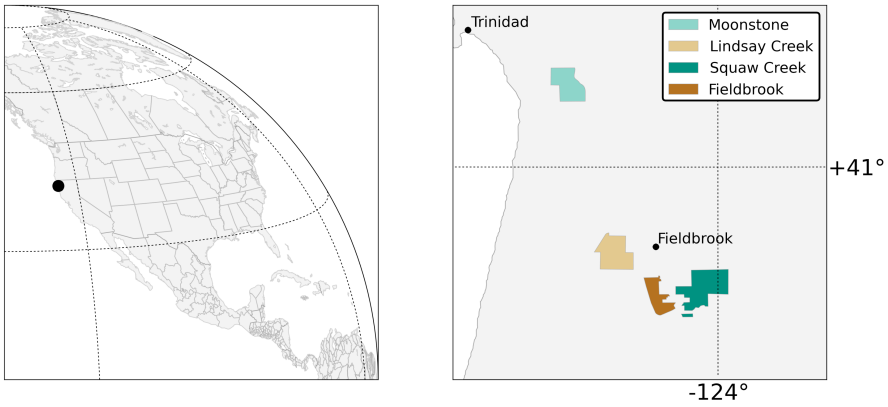

Figure 1: van Eck Study area location and management units.

2. Background

2.1 Detection and delineation

The majority individual tree identification methods using LiDAR data combine the creation of a Digital Surface Model (DSM) and Canopy Height Model (CHM) with Local Maxima (LM) filtering to identify tree locations (Jensen et al. 1987; Kaartinen et al. 2008; Lee et al. 2010; McCombs et al. June 2003; Tesfamichael et al. 2009, 2010). The efficacy of methods relying on LM filtering for tree detection depends on the determination of an analysis window size that reflects the crown area of the trees being identified. Popescu et al. (2002) tested an approach using a variable window defined by stand specific field data. However, this approach is dependent on field observation of crown radii to calibrate the LM window size.

Several methods have been tested to estimate tree crown and bole parameters (radius, bole volume, etc) once tree location has been established. Region growing methods such as the watershed delineation adapted from terrain analysis are common (Hyyppä et al. 2001; Schardt et al. 2002; Ziegler et al. 2000). Geometric models of tree crown shapes have also been used to delineate individual trees in Airborne Laser Scanning (ALS) data. Abstract tree crown form was first described by Horn (1971). The Horn equation has been modified and adapted to tree crown measurement from aerial photography and LiDAR (Gong et al. 2002; Holmgren et al. 2003; Pollock 1996; Sheng et al. 2001; Wolf and Heipke 2007). Persson (2001) and Persson et al. (2002) used a second order polynomial to choose between multiple candidate trees selected by multi-scale LM filtering. Andersen et al. (2002) used the shape proposed by Sheng et al. (2001) to predict crown shape using parameters derived from Bayesian probability analysis of points trained by the likelihood of points penetrating into a tree canopy as a result of their scan angle. Popescu et al. (2003) used a fourth order polynomial to determine crown diameter after a variable shape/radius LM filter (Popescu et al. 2002) was used to detect trees. Wack et al. (2003) used a conic section to identify points belonging to distinct trees. Falkowski et al. (2006) used

Spatial Wave Analysis (SWA), measuring goodness-of-fit of a 2-dimensional Ricker wavelet to the CHM resulting in location, crown radius, and height of individual trees within the coverage area. Wolf and Heipke (2007), Heurich (2008), and Kaartinen et al. (2008) utilized a variation on Pollock (1996) crown shape to aggregate wrongly identified individual crowns from small scale LM filtering as in Persson (2001).

2.2 RANSAC

RANSAC (Fischler and Bolles 1981) is a paradigm for fitting experimental data to a mathematical model. With sufficient point coverage, objects within a LiDAR scene may be reconstructed by interpolating a surface from points. The RANSAC approach has notable advantages over other approaches to canopy model fitting as it iteratively determines the best set of points fitting a model within the point cloud. It has been applied to the detection of objects from point clouds (Bretar and Roux 2005; Fontanelli et al. 2007; Forlani et al. 2003, 2006; Reitberger et al. 2007, 2009; Schnabel et al. 2007; Tarsha-Kurdi et al. 2007).

2.3 *StarSac*

The *StarSac* (Shafii et al. 2009) program was developed using RANSAC and Oliver Kreylos' Virtual Reality Toolkit (VRUI). We have revised *StarSac* and verify the results against those of a field survey. Unlike other projects, we use a modified version of RANSAC based upon a preliminary, fine scale local maxima filter to find tree canopies.

3. Methods

3.1 Field data collection

The forest consists of 4 tracts which were further divided into 21 stands ranging in size from 4 to 40 ha. Stand inventory was taken for standing live greater than 15.24 cm Diameter at Breast Height (1.37 m) (DBH). The primary objective of the inventory was to estimate total biomass and by extension total forest carbon. The variable plot method outlined in Dilworth and Bell (1963) was used. A Basal Area Factor (BAF) was selected for each stand prior to sampling to produce an average of 6 to 8 "in" trees per plot. Plots were spaced across each tract on a 50m x 100m grid. A total of 660 measure plots were installed.

3.2 Regression models

A regression model of the allometric relationship between height and DBH derived from field data was used to predict DBH from LiDAR derived tree heights. A general non-linear regression model for all species was used to establish DBH from height using measured trees from plots within the same stand. The equation used for regression analysis takes the standard form of:

$$DBH = a * H^{b} \qquad (1)$$

Where H is total tree height; a and b are spatially variable regression coefficients. ANAlysis Of VAriance (ANCOVA) was conducted to determine variation in regression coefficients among plots using the generalized linear model in the R statistical package (R Development Core Team 2008).

In Table 1, Model 1 establishes that the coefficients differ between stands, and Model 2 establishes that the slopes differ between stands.

Table 1: Analysis of deviance. Model 1: *log*(DBH) ~ stand + *log*(height), Model 2: *log*(DBH) ~ stand + stand * *log*(height).

Model	Resid. Df	Resid. Dev	Df	Deviance	P(>|Chi|)
1	1362	200.63			
2	1342	179.68	20	20.95	0.0000

Thus, regression coefficients were calculated for each stand and applied to the determination of DBH from LiDAR derived tree heights.

3.3 LiDAR data collection

LiDAR data were collected for 1796 ha on March 17th, 2008, conducted with an Optech 3100 sensor mounted in a Cessna Caravan 208B, with specifics shown in Table 2. Instrumentation was set to yield an average native pulse density of ≥ 6 pls/m^2 over terrestrial surfaces. The TerraScan® software suite was used to classify ground and non-ground points (Soninen 2004).

Table 2: Data Collection statistics.

Sensor	Optech 3100
Survey Altitude (AGL)	900 m
Pulse Rate	> 71 kHz
Pulse Mode	Single
Mirror Scan Rate	52 Hz
Field of View	28° (± from nadir)
Overlap	100% (50% Side-lap)

3.4 *StarSac*

The current RANSAC algorithm is summarized in pseudo-code below, with references to sections that explains key parts of the algorithm in greater detail.

1. For all locally maximal LiDAR points Max_i for i=1…n: (Section 3.4.1)
   (a) Find set of points around Max_i to create a fixed-size window.
   (b) For iterations j=1…T: (Section 3.4.2)
      i. Randomly select a subset of window points to create model M_j with Max_i as its peak, reject if shape is inappropriate. (Section 3.4.3)
      ii. Create consensus set C_j for M_j, determine radius. (Section 3.4.4)
      iii. If M_j has at most a (predefined) ratio of outliers to inliers, grade it and compare it with the best model M_{best}. Keep track of M_{best}. If no previous model was found then M_j is chosen as M_{best} assuming that its ratio of outliers to inliers is appropriate. (Section 3.4.5)
   (c) If M_{best} found, mark it.
2. Visualize canopy-approximating models as shaded surfaces for delineation. (Figure 10)
3. Calculate a height for each canopy-approximating model. (Section 3.4.6)

3.4.1 Local Maxima

Maximum points Max_i from first return points (classified as non-ground) are identified during pre-processing. Each maximum is selected based on the fact that it is higher than points inside of

a $1.5\,m \times 1.5\,m$ window centered on the maximum (see Figure 2). This small box is large enough to capture most peaks in our test data sets.

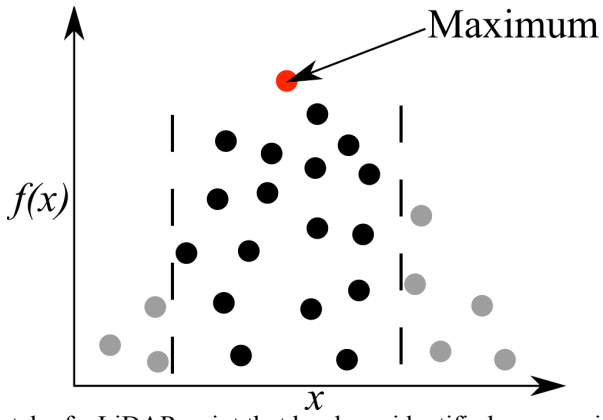

Figure 2: An artificial sketch of a LiDAR point that has been identified as a maximum where each point is defined by the one-dimensional function f(x). The maximum is higher than the other points inside of the box indicated by the dashed lines.

3.4.2 Number of Model Iterations

We calculate the number of RANSAC iterations T according to Schnabel et al. (2007), based on the probability that an appropriate model is found. If a window consists of N points, k points are used to instantiate our model. A good consensus set (i.e., inliers) consists of at least c points. The probability of finding an appropriate model in a single pass is:

$$P(c) = \frac{\binom{c}{k}}{\binom{N}{k}} \approx \left(\frac{c}{N}\right)^k \tag{2}$$

After picking s poor models, the probability of detecting an appropriate model is calculated by evaluating $P(c,s)$:

$$P(c,s) = 1 - (1 - P(c))^s \tag{3}$$

If we were to solve for s, we can calculate the number of candidates T required to detect shapes of size c with probability $P(c,T) \geq p_t$ as:

$$T \geq \frac{\ln(1 - p_t)}{\ln(1 - P(c))} \tag{4}$$

The denominator of (4) can be approximated by the Taylor series $\ln(1 - P(c)) = -P(c) + O(P(c)^2)$ and (4) can be written as:

$$T \approx \frac{-\ln(1 - p_t)}{P(c)} \tag{5}$$

We use (5) to define our number of iterations per window.

3.4.3 Model Creation

Our algorithm is currently capable of fitting a single type of model to the points of our data set. This model may be defined as a paraboloid, cone or "shape-shifter" shape. Each shape has a parameter defining its central peak (x_c, y_c, z_c) (defined by Max_i used to create the current window) and one parameter which controls its appearance. The paraboloid is defined by Equation (6) and is shown in Figure 3.

$$f(x,y) = a((x - x_c)^2 + (y - y_c)^2) + z_c \qquad (6)$$

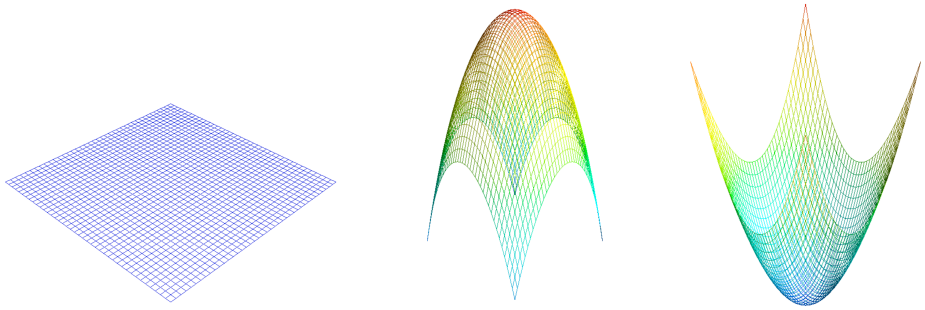

(a) Paraboloid with α=0.0. (b) Paraboloid with α=-1.0. (c) Paraboloid with α=1.0.

Figure 3: Renderings of the paraboloid with sample α values. Negative α values indicate a convex shape while positive α values indicate a concave shape.

If the α parameter is positive, the paraboloid is concave; if it is negative, it is convex. The cone is defined by Equation (7) and depicted in Figure 4.

$$f(x,y) = -\sqrt{\left(\frac{(x - x_c)^2 + (y - y_c)^2}{a}\right)} + z_c \qquad (7)$$

(a) Cone with α=0.1. (b) Cone with α=0.5.

Figure 4: Renderings of the cone using various values of α. The cone broadens as one increases α.

For the cone, α is always positive and causes the cone to broaden as it increases. Convex shapes resemble canopies; concave is seen as "inappropriate."

The shape-shifter (Equation 8) represents an interpolation between a cone and paraboloid. If α is zero, the shape is similar to a cone; if it is one, it resembles a paraboloid (Figure 5).

$$f(x,y) = -\alpha * ((x-x_c)^2 + (y-y_c)^2) + (a-1.0) * \sqrt{((x-x_c)^2 + (y-y_c)^2)} + z_c \qquad (8)$$

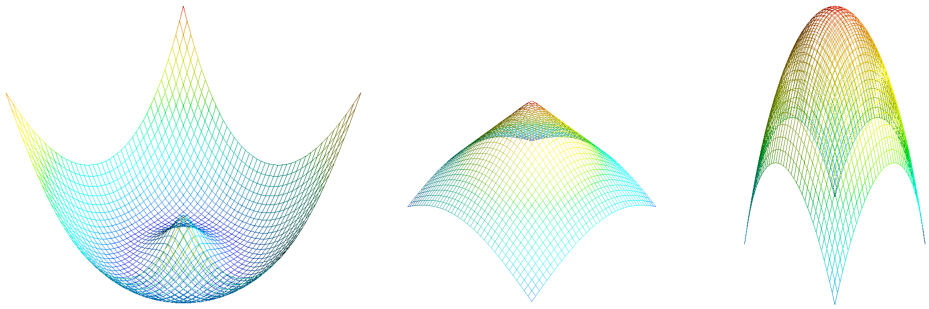

(a) Shape-shifter with α=-1.0. (b) Shape-shifter with α=0.0. (c) Shape-shifter with α=1.0.
Figure 5: Renderings of the shape-shifter (8) using various values of α. The valid range for α is 0-1.0, as an α value of -1.0 creates an unusual shape as shown in Figure 5.

3.4.4 Consensus Set

Each model's consensus set C_j is created by selecting points inside of the window which are identified as inliers. We assemble this set by first computing the $f(x, y)$ value for each window point and comparing that value with the point's z coordinate. If the different is smaller than a pre-defined error metric ε, the point is added to C_j.

After C_j is created, one can then calculate the radius by calculating the (two-dimensional, (x, y)) distance between the model's central peak and consensus point furthest from the peak.

3.4.5 Model Grading

In order to compare against other models, each model is graded by the number of inliers. The model with the best grade (most inliers) is identified in each window.

3.4.6 Tree height

To calculate the height for each tree, we use Hardy's multiquadric method (Hardy 1971) to reconstruct the ground surface beneath the tree crown. It is created by solving a system of n linear equations with n unknowns using ground points (x_i, y_i, z_i) where i=1,…,n, defined as follows:

$$\sum_{j=1}^{n} c_i \sqrt{((x_j - x_i)^2 + (y_j - y_i)^2} = z_i, i = 1, \ldots, n \qquad (9)$$

The quadric term c_i influences the shape of Equation (9). We then subtract the elevation of the hardy surface at the (x, y) location of the crown apex from the height (z-coordinate) of the crown apex.

3.5 LiDAR inventory

StarSac was run in a batch process over all LiDAR data in stands where field data was collected. The classified LAS files were subset into blocks containing ≈150,000 points. Each block was further subset into ground-only points and points classified as first return and vegetation. LiDAR

data was processed using the LibLAS (Loskot 2008) command line tools and application programming interface (API). *StarSac* output was collected in a PostgreSQL (The PostgreSQL Global Development Group 2005) relational database with the PostGIS (Holl and Plum 2009) spatial object extensions.

To test the accuracy of the tree identification method outlined above, "in" trees were identified from the LiDAR-derived trees based upon DBH, BAF, and distance to the nearest plot center used in the field inventory. Stand-specific, non-linear regression coefficients derived from field data were used to regress LiDAR-derived tree height to tree DBH. Once DBH was modeled, the status of all trees with regard to the BAF was assessed based upon the distance between the tree and the plot center. The maximum distance from a plot center that a tree with given DBH could be, is given as:

$$r = d * \sqrt{\left(\frac{10980}{BAF}\right) - 1} \tag{10}$$

where r is the plot radius (ft) for a given DBH (d in ft), and BAF (ft^2ac^{-1}) (See Dilworth and Bell (1963) for further explanation). Thus:

$$\begin{aligned} B_{tree} &= 0 \text{ if } \left|(x_{tree}, y_{tree}) - (x_{plot}, y_{plot})\right| > r_{tree} \\ B_{tree} &= 1 \text{ if } \left|(x_{tree}, y_{tree}) - (x_{plot}, y_{plot})\right| \leq r_{tree} \end{aligned} \tag{11}$$

where the binary value of B_{tree} identifies a tree as "in" or "out."

4. Results

4.1 Field inventory

The BAF selected for each plot resulted in between 5 and 8 trees per plot. Basal area ranges between 36 m^2ha^{-1} to 74 m^2ha^{-1} and generally varies with DBHq though with greater magnitude.

4.1.1 Regression models

The LiDAR methods employed here do not differentiate between species, thus regression coefficients were developed using all trees within a given stand. Figure 6 shows the general relationship between DBH and height by species in a 2D histogram. Visual inspection of Figure 7 indicates similarity between species, justifying the application of an approach that is not capable of differentiating between species, such as the *StarSac* method employed here.

Figures 8 and 9 represent the results of the regression of DBH and height for all field measured trees and for all measured trees and by stand respectively.

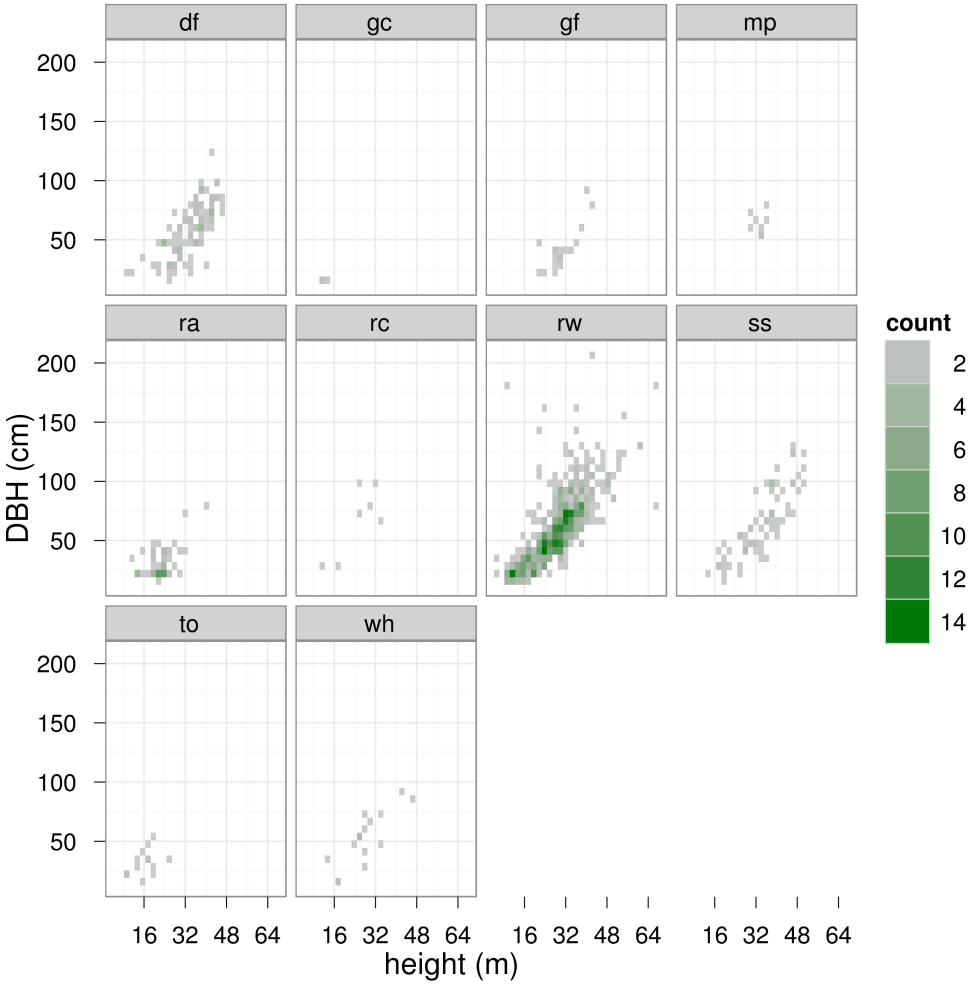

Figure 6: Two dimensional histogram. *df*, Douglas fir;*gf*, Grand; *mp*, big-leaf maple; *ra*, Red alder; *rc*, Western red cedar; *rw*, Coast redwood; *ss*, Sitka spruce; *to*, Tan oak; *wh*, Western hemlock.

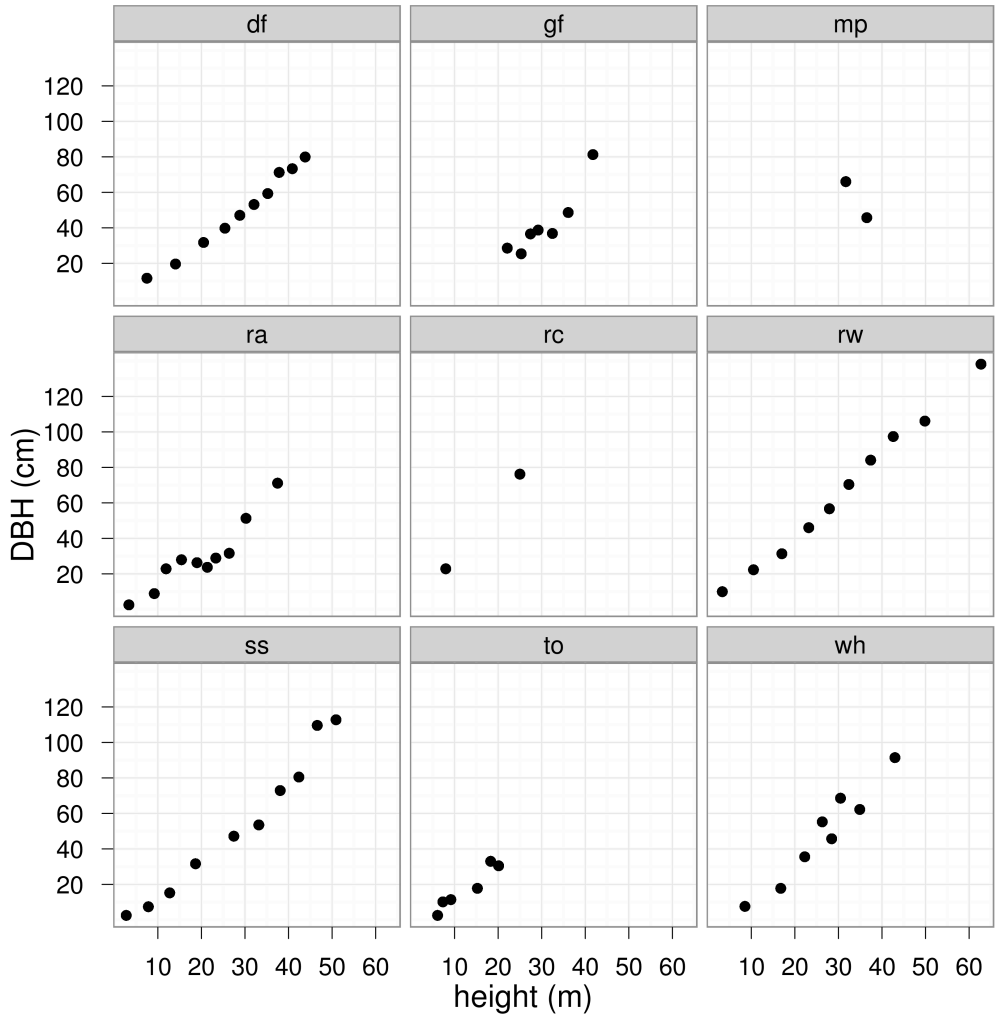

Figure 7: Average DBH within height bins. *df*, Douglas fir;*gf*, Grand; *mp*, big-leaf maple; *ra*, Red alder; *rc*, Western red cedar; *rw*, Coast redwood; *ss*, Sitka spruce; *to*, Tan oak; *wh*, Western hemlock.

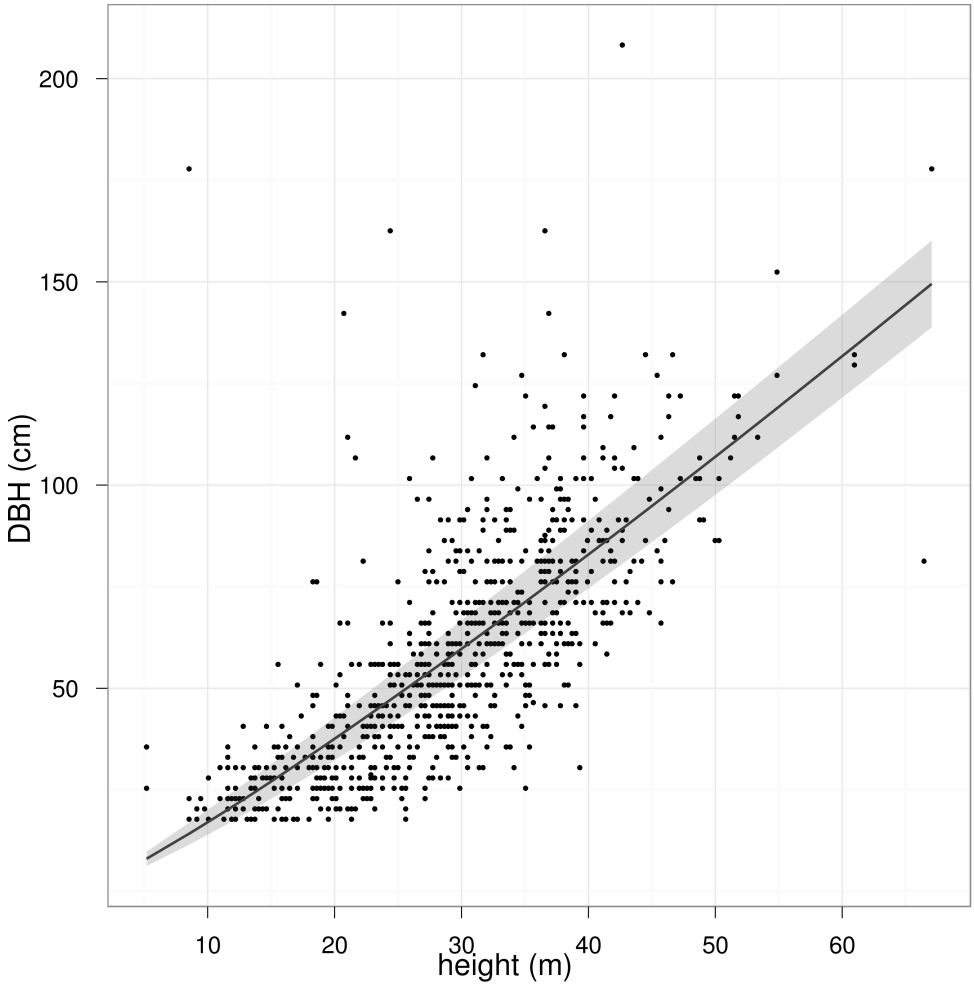

Figure 8: Height-DBH regression for all trees.

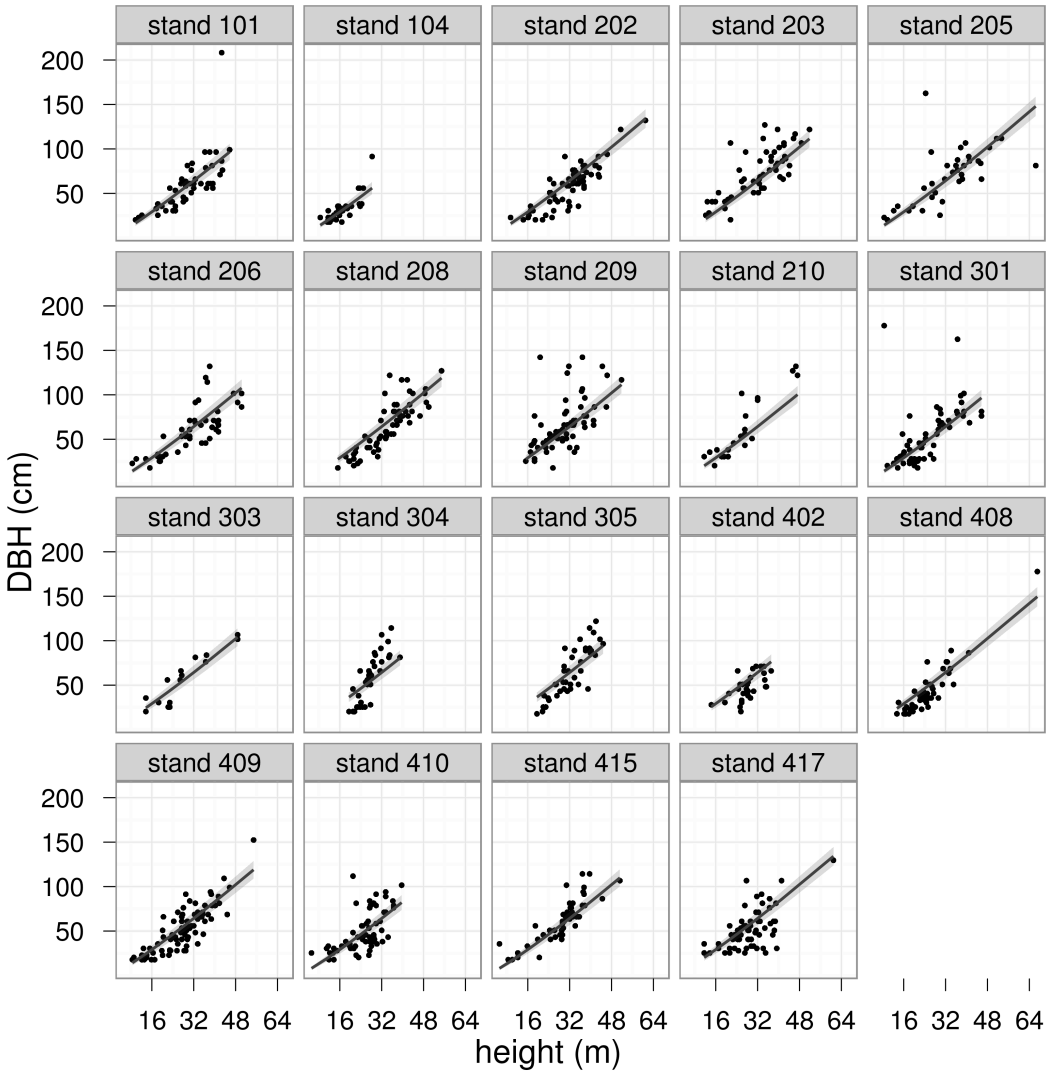

Figure 9: Height-DBH regression by stand. *df*, Douglas fir;*gf*, Grand; *mp*, big-leaf maple; *ra*, Red alder; *rc*, Western red cedar; *rw*, Coast redwood; *ss*, Sitka spruce; *to*, Tan oak; *wh*, Western hemlock.

4.2 LiDAR analysis

Individual tree identification using the RANSAC method was effective in most cases. Visual inspection of the consensus sets (Figure 10) identified was used extensively in testing the impact of changes to the approach.

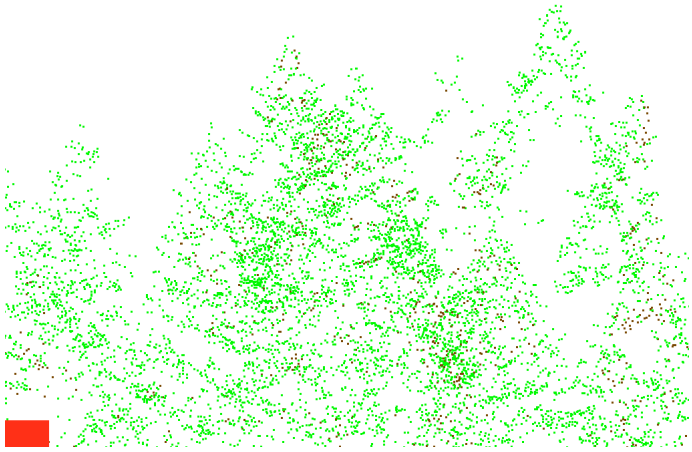

(a) Raw LiDAR points.

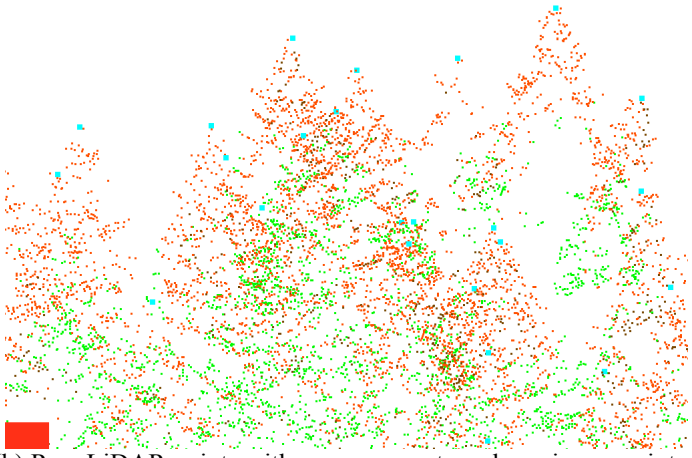

(b) Raw LiDAR points with consensus sets and maximum points.

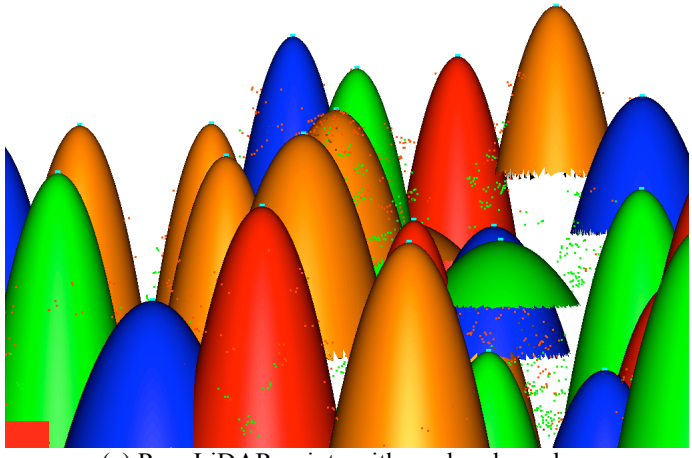

(c) Raw LiDAR points with rendered graphs.

Figure 10: An example of three-dimensional graphs that depict the models used to identify the canopies in StarSac. Each graph is created by using the model's equation and radius. The raw LiDAR rendering is showing in Figure 10(a). In Figure 10(b), central peak points are rendered as thick, cyan points and consensus set points are colored red. The resulting graphs of the canopies are shown in Figure 10(c).

4.3 LiDAR inventory

The LiDAR inventory method was compared with field methods for the determination of basal area. Stand-aggregated basal area estimates were derived using the basal area calculated for each plot. Figures 11 and 12 show the basal area and tree count comparison between methods.

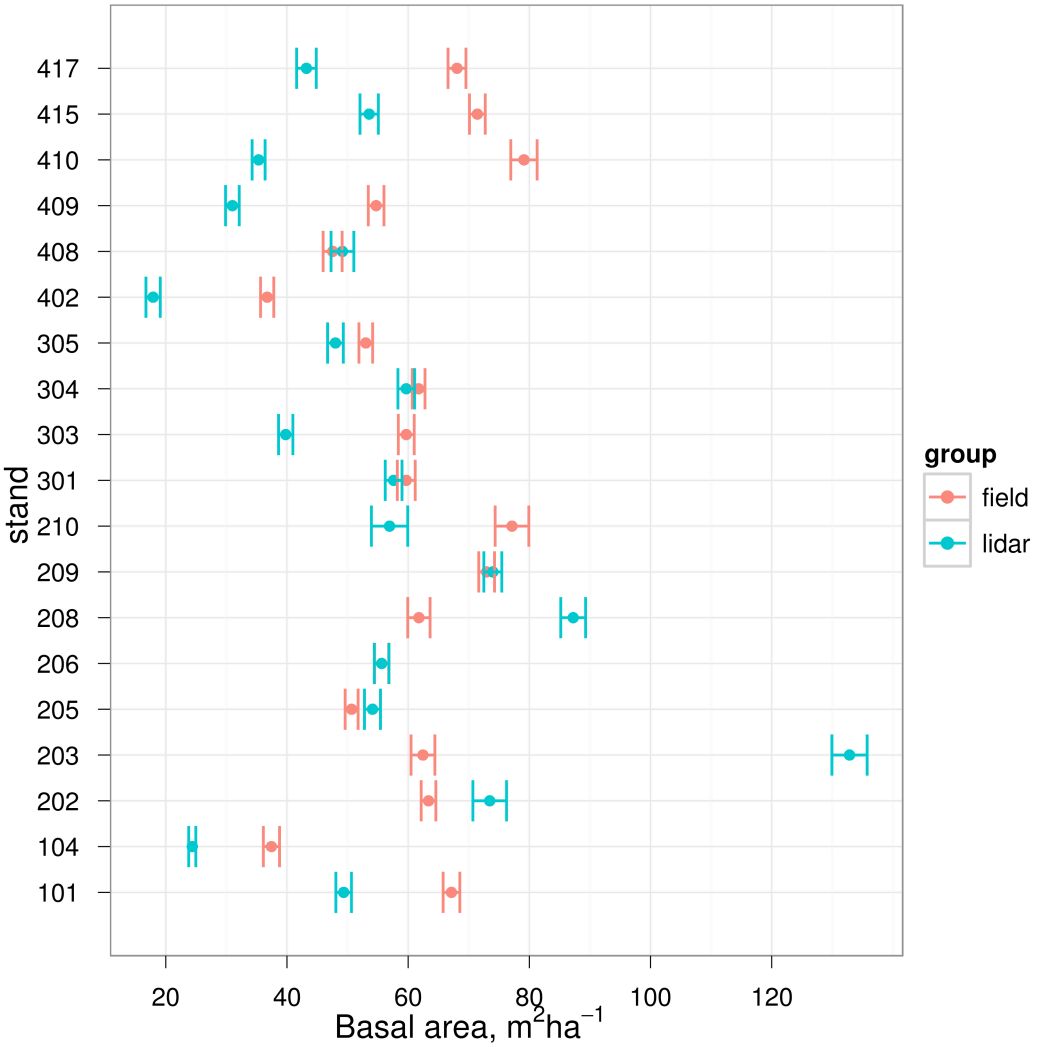

Figure 11: Average plot basal area comparison between LiDAR and field methods with 95% confidence interval whiskers.

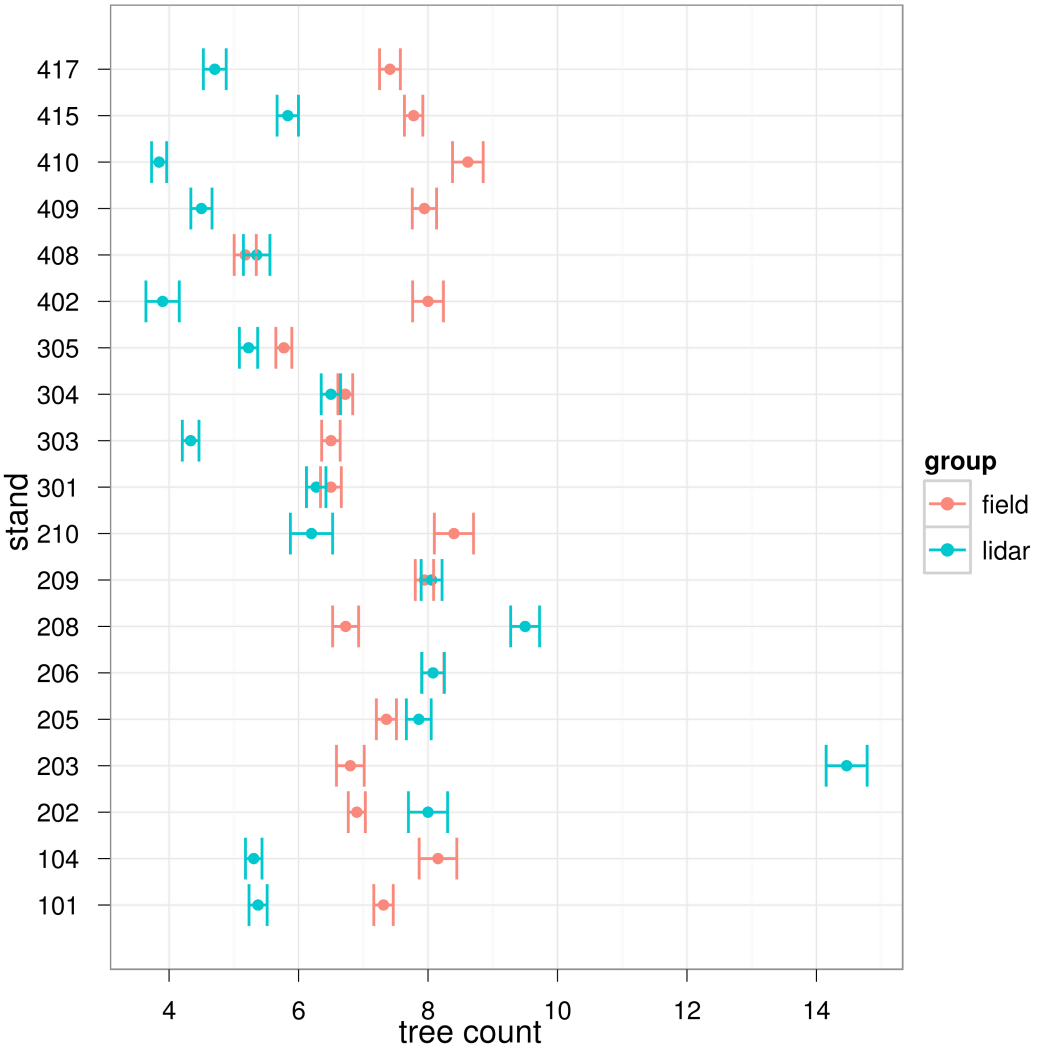

Figure 12: Average plot tree count comparison between LiDAR and field methods with 95% confidence interval whiskers.

Figure 13 indicates that the LiDAR method results in greater basal area estimation in the 50 cm to 125 cm DBH range while field methods estimate greater basal area in the 12 cm to 50 cm and 150 cm to 350 cm ranges.

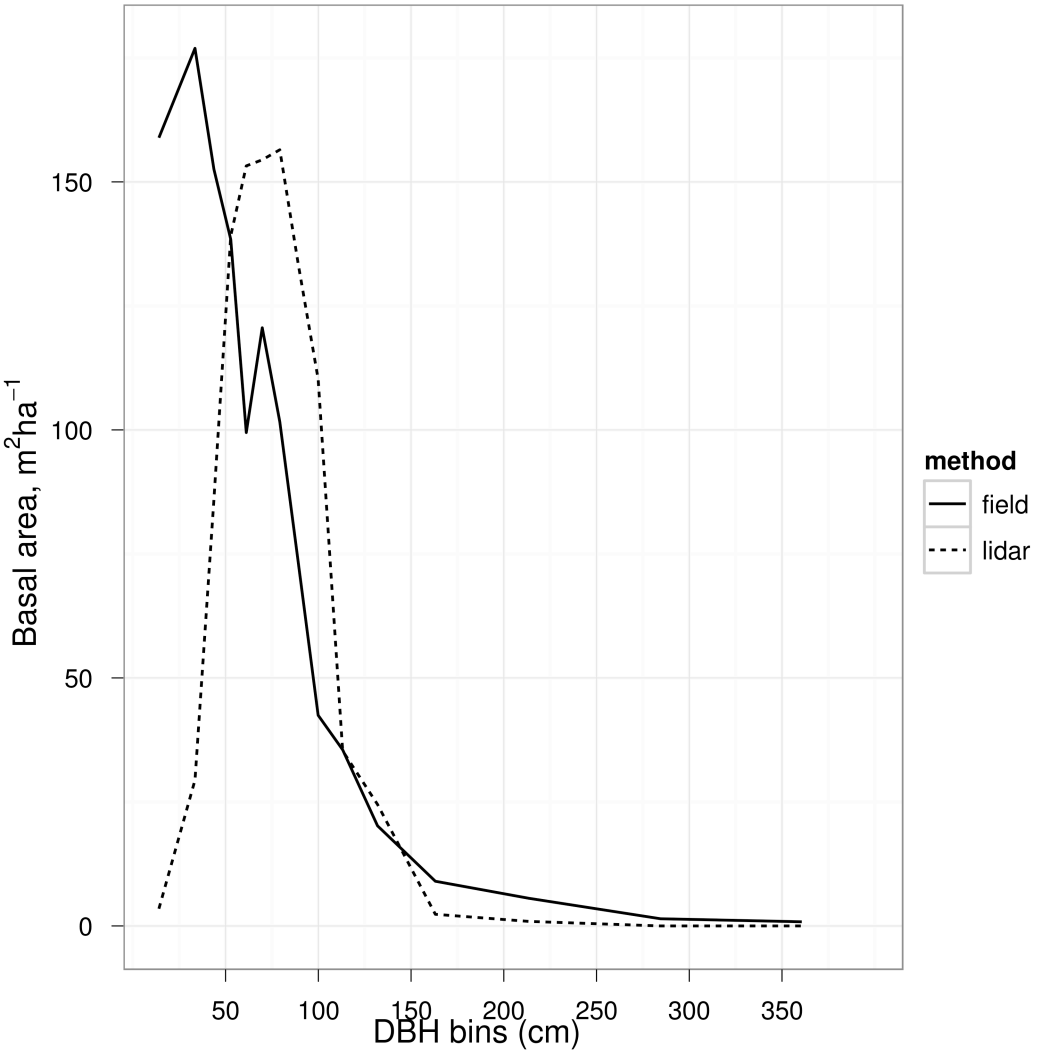

Figure 13: Density plot of basal area by DBH histogram bins for LiDAR and field methods.

The results show strong agreement in many stands while a few stands show some disparity. In general, field methods resulted in a higher tree count and greater basal area.

Table 3 shows tree count/plot averaged across all plots. While there are significant differences in the count and basal area between the LiDAR and field methods for given stands, the combined statistics indicate that the results of field and LiDAR methods are within a RMSD of less than 3.5 m^2ha^{-1} (see Table 4).

Table 3: Average plot tree count and basal area for all plots.

LiDAR count	Field count (average)	LiDAR basal area, m^2ha^{-1}	Field basal area, m^2ha^{-1} (average)
6.64	7.17	57.07	60.33

Table 4: Paired *t* test and RMSD for tree count and basal area for all plots..

df	Tree count *t*	Tree count P	BA[a] *t*	BA[a] P	Count RMSD	BA[a] RMSD
301	-1.807	0.072	-1.278	0.202	0.530	3.261

[a] basal area

Paired *t* test between LiDAR and field methods indicate that the means for all paired plots were not significantly different for tree counts (P=0.072) or basal area (P=0.202).

4.4 Factors affecting agreement between LiDAR and field measures

While overall differences between the methods are not significant, there is obviously some variation between the means for LiDAR and field methods for both tree count and basal area (Figures 12 and 11). As the van Eck forest stands were classified by canopy density and other factors, we can assess the impact of these generalized stand characteristics on the differences between the two measurement methods. This is accomplished using ANalysis Of VAriance (ANOVA) for the regression of the stand characteristics (*predictor*) and the log-transformed ratio of basal area estimates (*response*) from the two basal area estimation methods (Equation (12 in Wilkinson-Rogers notation).

$$lm\left[\log\left(\frac{BA_l}{BA_f}\right) \sim DBH_c * CanopyDensity_c\right] \quad (12)$$

A two-way ANOVA reveals that neither the interaction of canopy cover and DBH, or DBH alone has significant effects, but that canopy cover does have an impact upon the variation between measures (Table 5). A one-way ANOVA (Table 6) reveals that the variance in estimated basal area between methods is significant in stands classified in the 40-60% canopy coverage range. Levene's test reveals that the variance is homogeneous between canopy cover levels (Table 7), validating the assumptions in the one-way test.

Table 5: Two-way ANOVA test for the influence of canopy cover and DBH classification on variance between estimation methods.

	Df	Sum Sq	Mean Sq	F value	Pr(>F)
dbhmid	1	0.00	0.00	0.00	0.9972
densmid	1	5.81	5.81	8.59	0.0036
dbhmid:densmid	1	0.95	0.95	1.41	0.2361
Residuals	298	201.39	0.68		

Table 6: One-way ANOVA test for the influence of canopy cover on variance between estimation methods.

	Estimate	Std. Error	t value	Pr(>|t|)
(Intercept)	-0.1984	0.1390	-1.43	0.1547
densmid50	-0.7076	0.2949	-2.40	0.0170
densmid70	0.0702	0.1482	0.47	0.6359

Table 7: Levene's test of one-way ANOVA residuals from the influence of canopy cover on differences between basal area measures.

	Estimate	Std. Error	t value	Pr(>|t|)
(Intercept)	0.6413	0.0879	7.29	0.0000
densmid50	-0.0336	0.1865	-0.18	0.8571
densmid70	-0.0074	0.0937	-0.08	0.9375

Figure 14 shows the effect of canopy density on tree count and basal area estimation by LiDAR and Field methods. Mid-density stands (40%-60%) show significant variation in basal area estimates.

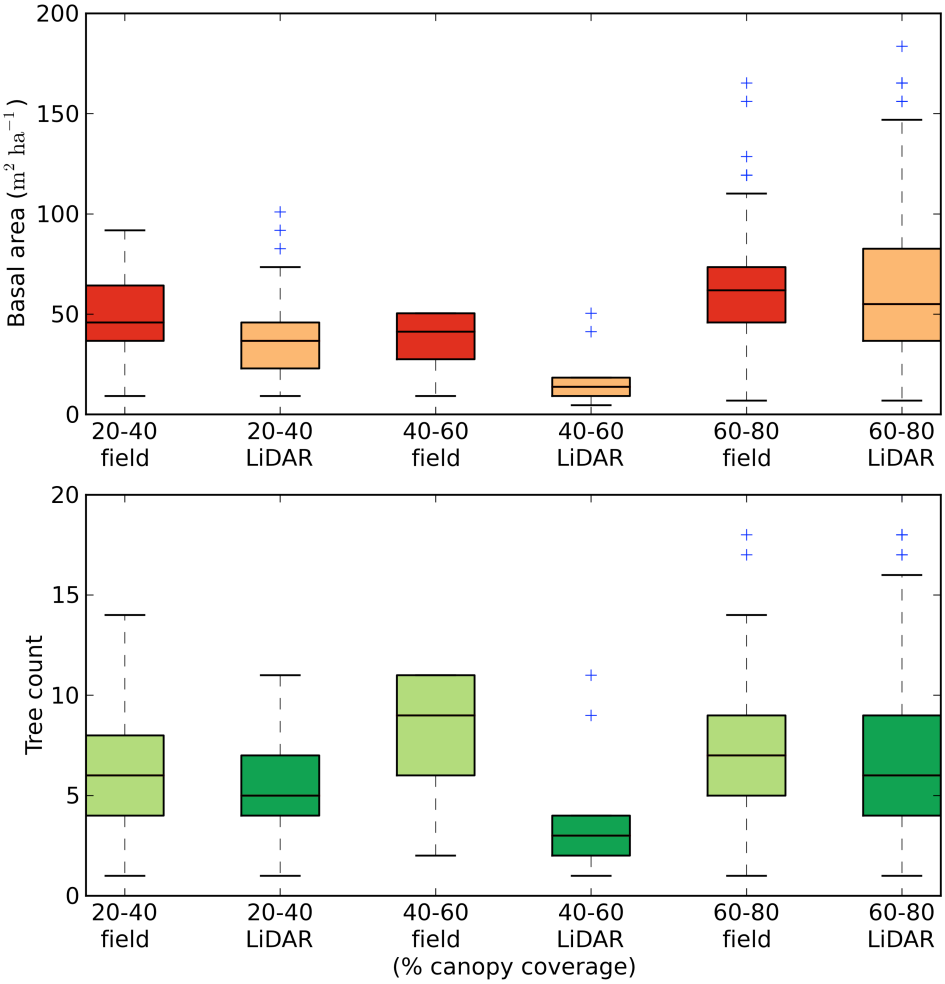

Figure 14: Variation between LiDAR and field based tree count and basal area estimates by percent canopy cover classes. Box extends from the lower to upper quartile values of the data, with a line at the median.

Diameter classes did not strongly influence differences in tree counts or basal area estimation by the two methods (Table 5). Figure 15 shows the variability between methods across the range of DBH classes. Figure 15 suggests that variation between basal area methods is greatest in the 0 cm to 20 cm DBH and 61 cm to 81 cm DBH classes.

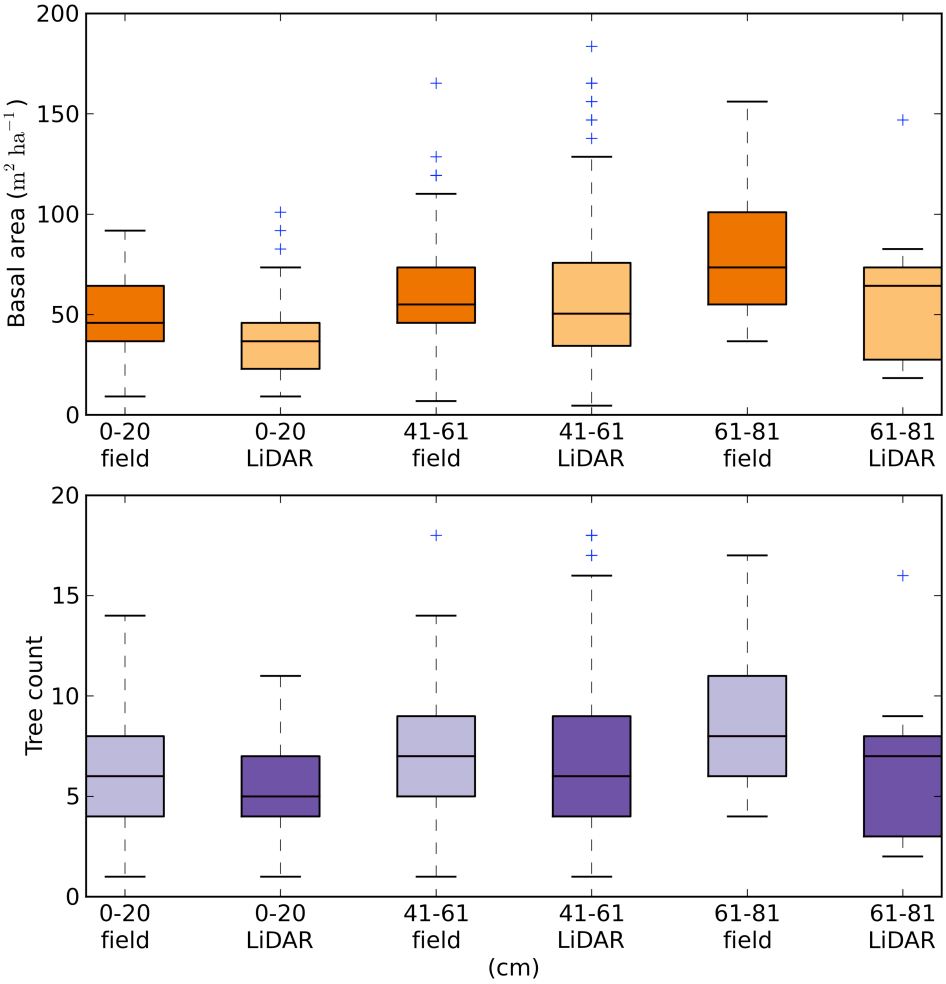

Figure 15: Variation between LiDAR and field based tree count and basal area estimates by diameter classification. Box extend from the lower to upper quartile values of the data, with a line at the median.

5. Conclusions, Future Research

This research gives insight into forest inventory from aerial LiDAR data across forest stands that are heterogeneous with regard to management history, species mix, and site characteristics. Tree detection and height estimation is accomplished without the use of regression models. The replication of a variable plot method was used so that results of field and LiDAR methods are comparable. The comparisons in Section 4 indicate that the tree identification and delineation-based LiDAR inventory method, applied to dense, mixed-species stands on variable terrain, yields similar tree count and basal area estimates to the field inventory method. The small difference between average basal area estimated by the two methods indicates that though some trees are not identified using the LiDAR method, they tend to be smaller trees and contribute less to the aggregate statistics.

The following summarizes the distinct contributions that this research makes.

- RANSAC approach to individual tree crown fitting reduces the need for extensive field data collection to parameterize detection.

- Geometric crown shape enables the identification of a range of crown shapes without unnecessary computation in structurally and ecologically diverse forest types.
- Local Maxima pre-filtering before RANSAC reduces unnecessary model testing.
- Detection is conducted on point data reducing the potential for compounding errors from gridded data analysis.

There exist multiple directions for future research. We intend on refining the RANSAC method such that LM filtering may be eliminated from the algorithm and the sub-canopy vegetation characteristics can be assessed as well. Additionally, we will investigate ways to incorporate methods identified in (Schnabel et al. 2007) for preliminary selection of model parameters using point normals. We hope to improve *StarSac* so that it may provide information about a range of structural measures relating to habitat, fire behavior, and forest health.

Acknowledgements

The authors would like to thank Oliver Kreylos for providing thoughtful commentary on the manuscript.

References

H.E. Andersen, S.E. Reutebuch, and G.F. Schreuder. Bayesian object recognition for the

analysis of complex forest scenes in airborne laser scanner data. *International Archives of Photogrammetry, Remote Sensing, and Spatial Information Sciences*, 34(3/A):35–41, 2002. ISSN 1682-1750.

F. Bretar and M. Roux. Hybrid image segmentation using LiDAR 3D planar primitives. In *Laser scanning 2005*, pages 12–14. ISPRS, 2005.

J.R. Dilworth and J.F. Bell. *Variable plot cruising*. OSU Book Stores, 1963.

M.J. Falkowski, A.M.S. Smith, A.T. Hudak, P.E. Gessler, L.A. Vierling, and N.L. Crookston. Automated estimation of individual conifer tree height and crown diameter via two-dimensional spatial wavelet analysis of lidar data. *Canadian Journal of Remote Sensing*, 32(2): 153–161, 2006.

Martin A. Fischler and Robert C. Bolles. Random sample consensus: a paradigm for model fitting with applications to image analysis and automated cartography. *Commun. ACM*, 24:381–395, June 1981. ISSN 0001-0782. URL `http://doi.acm.org/10.1145/358669.358692`.

D. Fontanelli, L. Ricciato, and S. Soatto. A fast ransac-based registration algorithm for accurate localization in unknown environments using lidar measurements. In *IEEE International Conference on Automation Science and Engineering, 2007. CASE 2007*, pages 597–602, 2007.

G. Forlani, C. Nardinocchi, M. Scaioni, and P. Zingaretti. Building reconstruction and visualization from LIDAR data. *INTERNATIONAL ARCHIVES OF PHOTOGRAMMETRY REMOTE SENSING AND SPATIAL INFORMATION SCIENCES*, 34(5/W12):151–156, 2003. ISSN 1682-1750.

G. Forlani, C. Nardinocchi, M. Scaioni, and P. Zingaretti. Complete classification of raw LIDAR data and 3D reconstruction of buildings. *Pattern Analysis & Applications*, 8(4): 357–374, 2006. ISSN 1433-7541.

P. Gong, Y. Sheng, and G.S. Biging. 3D Model-based tree measurement from high-resolution aerial imagery. *Photogrammetric engineering and remote sensing*, 68 (11):1203–1212, 2002. ISSN 0099-1112.

Rolland L. Hardy. Multiquadric equations of topography and other irregular surfaces. *J. Geophys. Res.*, 76(8):1905–1915, 1971. ISSN 0148-0227. 10.1029/JB076i008p01905. URL http://dx.doi.org/10.1029/JB076i008p01905.

Marco Heurich. Automatic recognition and measurement of single trees based on data from airborne laser scanning over the richly structured natural forests of the bavarian forest national park. *Forest Ecology and Management*, 255(7):2416 – 2433, 2008. ISSN 0378-1127. URL http://www.sciencedirect.com/science/article/B6T6X-4S02JX3-1/2/453e6ff86a62cf2643f94d558cfaff71. Large-scale experimentation and oak regeneration.

Stephan Holl and Hans Plum. PostGIS. *GeoInformatics*, 03/2009:34–36, April 2009. URL http://fluidbook.microdesign.nl/geoinformatics/03-2009/?page=34.

J. Holmgren, M. Nilsson, and H. Olsson. Estimation of tree height and stem volume on plots using airborne laser scanning. *Forest Science*, 49:419–428(10), 2003. URL http://www.ingentaconnect.com/content/saf/fs/2003/00000049/00000003/art00009.

H.S. Horn. *The adaptive geometry of trees*. Princeton Univ Pr, 1971. ISBN 0691023557.

J. Hyyppä, O. Kelle, M. Lehikoinen, and M. Inkinen. A segmentation-based method to retrieve stem volume estimates from 3-d tree height models produced by laser scanners. *Geoscience and Remote Sensing, IEEE Transactions on*, 39(5):969 –975, May 2001. ISSN 0196-2892.

John R. Jensen, Michael E. Hodgson, Halkard E. Mackey, and William Krabill. Correlation between aircraft mss and lidar remotely sensed data on a forested wetland. *Geocarto International*, 2(4):39–54, 1987.

H. Kaartinen, J. Hyyppä, X. Liang, P. Litkey, A. Kukko, X. Yu, H. Hyyppä, and M. Holopainen. Accuracy of automatic tree extraction using airborne laser scanner data. *SilviLaser*, 2008:8th, 2008.

Oliver Kreylos. Vrui vr, 2011. URL http://idav.ucdavis.edu/ okreylos/ResDev/Vrui/index.html. v2.0.

H. Lee, KC Slatton, BE Roth, and WP Cropper. Adaptive clustering of airborne LiDAR data to segment individual tree crowns in managed pine forests. *International Journal of Remote Sensing*, 31 (1):117–139, 2010. ISSN 0143-1161.

Mateusz Loskot. Introduction to asprs las data processing with liblas. In *FOSS4G 2008*, 2008. URL http://www.osgeo.org/ocs/index.php/foss4g/2008/paper/view/362.

J.W. McCombs, S.D. Roberts, and D.L. Evans. Influence of fusing lidar and multispectral imagery on remotely sensed estimates of stand density and mean tree height in a managed loblolly pine plantation. *Forest Science*, 49:457–466(10), June 2003. URL http://www.ingentaconnect.com/content/saf/fs/2003/00000049/00000003/art00013.

A. Persson, J. Holmgren, and U. Soderman. Detecting and measuring individual trees using an airborne laser scanner. *PE & RS- Photogrammetric Engineering & Remote Sensing*, 68(9):925–932, 2002. ISSN 0099-1112.

Åsa Persson. Extraction of individual trees using laser radar data. Master's thesis, Chalmers University of Technology, Department of Signals and Systems, Göteborg, Sweden,, 2001.

Richard James Pollock. *The automatic recognition of individual trees in aerial images of forests based on a synthetic tree crown image model*. PhD thesis, University of British Colombia, 1996.

S.C. Popescu, R.H. Wynne, and R.F. Nelson. Measuring individual tree crown diameter with lidar and assessing its influence on estimating forest volume and biomass. *Canadian Journal of Remote Sensing*, 29(5): 564–577, 2003.

Sorin C. Popescu, Randolph H. Wynne, and Ross F. Nelson. Estimating plot-level tree heights with lidar: local filtering with a canopy-height based variable window size. *Computers and Electronics in Agriculture*, 37 (1-3):71 – 95, 2002. ISSN 0168-1699. URL http://www.sciencedirect.com/science/article/B6T5M-478RN2H-6/2/55e9624eb4068f98ed9e04011f1d74fc.

R Development Core Team. *R: A Language and Environment for Statistical Computing*. R Foundation for Statistical Computing, Vienna, Austria, 2008. URL http://www.R-project.org. ISBN 3-900051-07-0.

J. Reitberger, P. Krzystek, and U. Stilla. Combined tree segmentation and stem detection using full waveform lidar data. *International Archives of Photogrammetry, Remote Sensing and Spatial Information Sciences*, 36:332–337, 2007.

J. Reitberger, C. Schnorr, P. Krzystek, and U. Stilla. 3D segmentation of single trees exploiting full waveform LIDAR data. *ISPRS Journal of Photogrammetry and Remote Sensing*, 64(6):561–574, 2009.

M. Schardt, M. Ziegler, A. Wimmer, R. Wack, and J. Hyyppä. Assessment of forest parameters by means of laser scanning. *International Archives of Photogrammetry, Remote Sensing, and Spatial Information Sciences*, 34(3/A,):302–309, 2002. ISSN 1682-1750.

R. Schnabel, R. Wahl, and R. Klein. Efficient ransac for point-cloud shape detection. *Computer Graphics Forum*, 26(2):214–226, 2007. ISSN 1467-8659. URL http://dx.doi.org/10.1111/j.1467-8659.2007.01016.x.

S. Shafii, B. Hamann, R. Hutchison, O. Kreylos, and J. Viers. Tree Detection and Delineation of the Consumnes River Preserve. In B.G. Lees and S.W. Laffan, editors, *10th International Conference on GeoComputation*, Sydney, November-December 2009. University of New South Wales.

Y. Sheng, P. Gong, and GS Biging. Model-based conifer-crown surface reconstruction from high-resolution aerial images. *PE & RS- Photogrammetric Engineering and Remote Sensing*, 67(8):957–965, 2001. ISSN 0099-1112.

A. Soninen. *TerraScan User's Guide*. Terrasolid, 2004.

F. Tarsha-Kurdi, T. Landes, and P. Grussenmeyer. Hough-transform and extended RANSAC algorithms for automatic detection of 3D building roof planes from Lidar data. *International Archives of Photogrammetry, Remote Sensing and Spatial Information Sciences*, 36(3/W52):407–412, 2007.

S.G. Tesfamichael, F. Ahmed, J.A.N. van Aardt, and F. Blakeway. A semi-variogram approach for estimating stems per hectare in eucalyptus grandis plantations using discrete-return lidar height data. *Forest Ecology and Management*, 258(7):1188 – 1199, 2009. ISSN 0378-1127. URL http://www.sciencedirect.com/science/article/B6T6X-4WMD2J9-4/2/a11ab87a82802ef1a61ccde32fe2ea43.

S.G. Tesfamichael, J.A.N. van Aardt, and F. Ahmed. Estimating plot-level tree height and volume of eucalyptus grandis plantations using small-footprint, discrete return lidar data. *Progress in Physical Geography*, 34(4): 515–540, 2010. URL http://ppg.sagepub.com/content/34/4/515.abstract.

The PostgreSQL Global Development Group. Postgresql 8.1.4 documentation, 2005. URL http://www.postgresql.org/docs/manuals/.

P. Torr and A. Zisserman. MLESAC: A new robust estimator with application to estimating image geometry. *Computer Vision and Image Understanding*, 78 (1):138–156, 2000.

R. Wack, M. Schardt, U. Lohr, L. Barrucho, and T. Oliveira. Forest inventory for eucalyptus plantations based on airborne laserscanner data. *The International Archives of the Photogrammetry, Remote Sensing and Spatial Information Sciences*, 2003.

Bernd-Michael Wolf (né Straub) and Christian Heipke. Automatic extraction and delineation of single trees from remote sensing data. *Machine Vision and Applications*, 18:317–330, 2007. ISSN 0932-8092. URL http://dx.doi.org/10.1007/s00138-006-0064-9. 10.1007/s00138-006-0064-9.

Michaela Ziegler, Harald Konrad, Johannes Hofrichter, Andreas Wimmer, Georg S. Ruppert, Mathias Schardt, and Juha M. Hyyppä. As sessment of forest attributes and single-tree segmentation by means of laser scanning. In Gary W. Kamerman, Upendra N. Singh, Christian Werner, and Vasyl V. Molebny, editors, *Topography, Altimetry, and Vegetation Monitoring Systems*, volume 4035, pages 73–84. SPIE, 2000. 10.1117/12.397780. URL http://link.aip.org/link/? PSI/4035/73/1.